Molecular Insights for the Optimization of Solvent-Based Selective Extraction of Ethanol From Fermentation Broths

Samuel J. Keasler, John L. Lewin, and J. Ilja Siepmann
Depts. of Chemistry and of Chemical Engineering and Materials Science and the Chemical Theory Center, University of Minnesota, 207 Pleasant St. SE, Minneapolis, MN 55455

Nicole M. Gryska
Depts. of Chemistry and of Chemical Engineering and Materials Science and the Chemical Theory Center, University of Minnesota, 207 Pleasant St. SE, Minneapolis, MN 55455

Corporate Research Materials Laboratory, 201-2E-23, 3M Co., St. Paul, MN 55144

Richard B. Ross, Nathan E. Schultz, and Masayuki Nakamura
Corporate Research Materials Laboratory, 201-2E-23 3M Co., St. Paul, MN 55144

DOI 10.1002/aic.14055
Published online April 1, 2013 in Wiley Online Library (wileyonlinelibrary.com)

Simulations and experiments were carried out to explore the solvent extraction of ethanol from aqueous solution using a series of seven 10-carbon alcohols. It is shown that configurational-bias Monte Carlo simulations in the Gibbs ensemble coupled with the TraPPE-UA force field can be utilized for predictive screening of the different extraction abilities (in terms of capacity factor and selectivity) of these alcohols. Analysis of the simulation trajectories indicates that extraction capacity is connected to the stabilization of larger ethanol/water cluster in the organic solvent, whereas selectivity is improved when smaller ethanol/water clusters are more prevalent. © 2013 American Institute of Chemical Engineers *AIChE J*, 59: 3065–3070, 2013
Keywords: biofuel, fermentation, liquid-liquid extraction Monte Carlo simulation, aqueous solution

Introduction

The separation of ethanol and other high-value chemicals from fermentation broths has long been recognized as one of the biggest obstacles to its economical use as a renewable fuel source and chemical feedstock.[1–7] In the case of ethanol, distillation is currently the most common approach, but its high-energy requirement makes the search for alternative processes an extremely important area of energy research.

One alternative to distillation is liquid-liquid extraction followed by a second, less energy intensive process to remove the ethanol from the extracting fluid. Several publications have examined the ability of various organic solvents and mixtures to extract ethanol from aqueous solution.[8–13] High-molecular-weight, aliphatic alcohols have been proposed as promising candidates for this purpose.

An effective solvent for ethanol extraction needs to possess two important qualities. The first is a high capacity factor for ethanol, which is frequently expressed in terms of the distribution coefficient K_{DE}

$$K_{DE} = \frac{[EtOH]_{org}}{[EtOH]_{aq}}$$

where $[EtOH]_{org}$ and $[EtOH]_{aq}$ are the concentrations of ethanol in the organic and aqueous phases, respectively, and are usually expressed in terms of mass fractions.[14] The second important quality of an effective extraction fluid is a high selectivity for ethanol over water. This property is usually expressed in terms of the separation factor α[14]

$$\alpha = \frac{K_{DE}}{K_{DW}}$$

where K_{DW} is defined analogously to K_{DE}. Large values of the separation factor indicate that the solvent preferentially extracts ethanol over water. Thus, the ideal solvent would have large values for both K_{DE} and α, but a high K_{DE} is usually coupled to a low α and vice versa. Other extractant properties that influence the selection, but that are not considered here, are low solubility in the broth, low toxicity, low reactivity, ease of separation of the extracted ethanol, and cost.

Stephenson et al.[15,16] have performed molecular dynamics simulations for neat solvents in an attempt to understand the structural features that may lead to effective extraction of ethanol. They observed that the number of hydroxyl groups in the second and third solvation shells for neat alcohols correlates with the extraction efficiency when the molecular weight M_W, is similar, but that this correlation is weaker than

Additional Supporting Information may be found in the online version of this article.

Correspondence concerning this article should be addressed to J. I. Siepmann at siepmann@umn.edu.

the previously observed simple correlation to the molecular weight of the solvent (i.e., $1000/M_W$). Despite these efforts, the picture of how structural details can affect extraction efficiency remains incomplete.

Monte Carlo simulations of phase equilibria in the Gibbs ensemble[17–19] combined with configurational-bias Monte Carlo (CBMC) moves[20–23] have become routine for the computation of vapor–liquid equilibria. This approach has also been applied to the prediction of octanol-water partitioning[24] and retention in reversed-phase liquid chromatography[25] where in both cases the solutes are at infinite dilution. Here, we applied this technique to calculate extraction efficiencies in seven 10-carbon alcohols and examine the underlying structures at finite concentration of the ethanol solute.

Simulation and Experimental Details

The extractants investigated were seven 10-carbon alcohols, including decan-1-ol, decan-2-ol, decan-3-ol, decan-4-ol, 2-methylnonan-2-ol (2M2N), 3,7-dimethyloctan-3-ol (37DM3O), and 4-propylheptan-4-ol (4P4H).

The simulations were performed using the *NpT* Gibbs ensemble Monte Carlo approach[17–19] ($T = 298$ K and $p = 0.1$ MPa), and utilized three thermodynamically connected simulation boxes: an aqueous (water-rich) phase, a 10-carbon alcohol (organic-rich) phase, and a vapor phase (to increase the rate of particle transfers between the two liquid phases). Chemical equilibrium was maintained by transferring particles between the phases,[17–19] while mechanical equilibrium with a constant external pressure bath was maintained by performing volume moves on each of the simulation boxes individually. The remaining degrees of freedom were sampled using translational, rotational, and conformational moves. Since some of the molecules possess a branched topology, the coupled-decoupled (CD) CBMC algorithm[23] was employed during particle transfer and partial regrowth (conformational) moves. The particle transfer rate was also enhanced through the use of CD—CBMC identity switch[26,27] moves which enable the performance of swap moves for smaller molecules (for which the acceptance rate is relatively high) followed by conversion to larger, more difficult to swap molecules, e.g., a methanol molecule is converted to an ethanol molecule in one phase and an ethanol molecule is converted to methanol in another phase.

In a Gibbs ensemble simulation, one can only specify the total number of molecules of each type (that can distribute over the different simulation boxes), but not the equilibrium composition for a given phase. Here, the entire three-box system contained a total of 864 water molecules, 240 10-carbon alcohol molecules, two methanol molecules (used for the identity switch moves), a variable number of ethanol molecules, and 25 helium atoms. The number of ethanol molecules to be used for a system with a particular 10-carbon alcohol was adjusted throughout a long pre-equilibration period to yield an aqueous ethanol weight fraction within the range from 9.5 to 11 wt %, i.e., a larger number of ethanol molecules is needed for solvents with a larger K_{DE}. The weight fraction range is close to the concentration range found in the experimental setup after the ethanol molecules distributed between the two phases. The number of helium atoms was selected to yield a vapor-phase volume ($p = 0.1$ MPa) that is sufficient to contain on average slightly more than one water molecule and one ethanol molecule.

It was assumed that the solubility of the 10-carbon alcohols in water was negligible and swap/identity switch moves were not performed on these molecules. Helium atoms were likewise restricted to the vapor phase. For the rest of the molecules, move types were selected randomly with a probability of 0.002 for volume moves, 0.098 for CD—CBMC identity switch moves, 0.4 for CD—CBMC particle swap moves, 0.1 for CD—CBMC regrowth moves, 0.2 for translational moves, and 0.2 for rotational moves. The maximum displacements for translational, rotational, and volume moves were adjusted to give an acceptance rate of 50%.

The interactions of the water and alcohol molecules were represented by the TIP4P and TraPPE-UA force fields with Lorentz-Berthelot combining rules for all unlike Lennard-Jones interactions,[28–30] a combination that was previously found to yield very accurate infinite-dilution transfer free energies for partitioning between organic and aqueous phases.[31–33] Analytical tail corrections[34] were added for Lennard-Jones interactions beyond a cutoff of 14 Å in the liquid phases, and 30 Å in the vapor phase. Electrostatic interactions were treated using an Ewald summation[34] with a real space cutoff of 14 Å and $\kappa = 0.26$ in the liquid phases (30 Å, $\kappa = 0.09$ in the vapor phase).

For each type of solvent molecule, eight independent simulations were performed to estimate the statistical uncertainties that are given as the standard error of the mean. Following the pre-equilibration period during which the number of ethanol molecules was adjusted, an equilibration period of 200,000 Monte Carlo cycles was used for each independent simulation, where a Monte Carlo cycle consists of N Monte Carlo moves, and N is the total number of particles in the system. The production periods consisted of 250,000 Monte Carlo cycles for each independent simulation. Using the in-house MCCCS—MN software, 20,000 Monte Carlo cycles can be completed in 24 h on a single 2.8 GHz Intel Xeon X5560 processor (i.e., the total CPU time required for the production periods of 8 independent simulations for a given 10-carbon alcohol was 2400 h, but independent simulations and different 10-carbon alcohol systems were run in parallel).

A series of extraction experiments was also carried out to measure the equilibrium constants and separation factors for the seven extraction solvents so that the simulation predictions can be validated with a set of experimental data performed at the same conditions. 2 mL of 12 wt % ethanol solution in water was transferred to a 6 mL glass vial. 2 mL of one solvent was added to the ethanol solution in the vial, and then the vial was shaken vigorously for 10 min with a vertical shaker to thoroughly mix the contents. After shaking, the sample was incubated at 25°C overnight. After the incubation, 1-mL samples from the aqueous and solvent phases were collected and analyzed by gas chromatography (HP 6890 system) equipped with a thermal conductivity detector and a wax column (DB-WAX, J&W Scientific) to quantify ethanol and water concentrations in both phases. Extraction measurements were done in triplicate and the standard deviation of the data is about 3%.

Results and Discussion

The K_{DE} and α values obtained from the simulations are shown as a function of the experimental values in Figure 1. For perfect agreement between simulation and experiment, the data would lie on a line with a slope of unity and an intercept of zero. As indicated by least-squares fits, the absolute values for K_{DE} and α and the dynamical range for K_{DE} are overestimated by the simulations. However, the experimental ordering

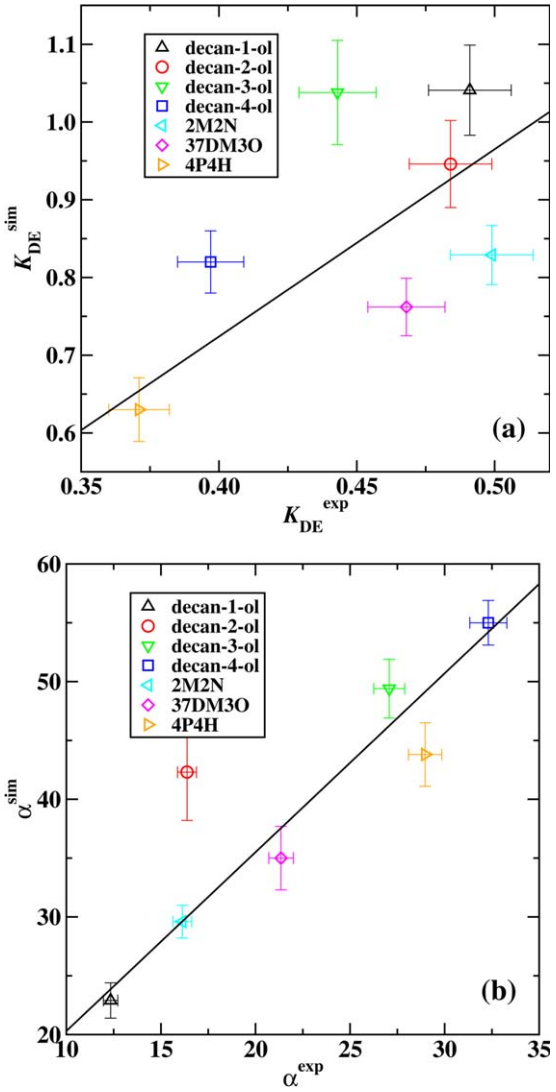

Figure 1. Comparison of K_{DE} (panel a) and α (panel b) values predicted from simulation and measured experimentally.

The dashed lines represent weighted linear least squares fits: $y = (-0.2 \pm 0.2) + (2.4 \pm 0.5)x$ (for K_{DE}), and $y = (5 \pm 3) + (1.5 \pm 0.2)x$ (for α). [Color figure can be viewed in the online issue, which is available at wileyonlinelibrary.com.]

of the different extraction solvents, both for K_{DE} and α, is well reproduced by the simulation data. The scatter in α is somewhat smaller, but this could be related to its larger dynamical range. It should be noted that an over prediction of K_{DE} by a factor of 1.5 corresponds to an error of only 1 kJ/mol in the transfer free energy.

The simulations correctly capture the decline in K_{DE} from decan-1-ol, over decan-2-ol to decan-4-ol (but the value for decan-3-ol is over predicted), and both the simulation and experiment predict the lowest K_{DE} value for 4P4H. Furthermore, both the simulations and experiments put the branched alcohols in the descending order of 2M2N, 37DM3O, and 4P4H. The major discrepancy in the ordering of the K_{DE} values is the relative values of the linear and branched alcohols. The simulation data for all alcohols with linear backbone lie above the best-fit line, whereas those for the branched alcohols fall below.

The ordering of the separation factors α is also predicted quite accurately. For the primary and secondary alcohols, the simulations correctly predict that the α values increase from decan-1-ol to decan-4-ol, and the trend within the series of tertiary alcohols is also reproduced. The simulations correctly place 2M2N between decan-1-ol and decan-2-ol, but somewhat under predict the α values of the other two tertiary alcohols and overpredict the value for decan-2-ol.

Another difference is that the simulations yield an α value for decan-2-ol that is closer to that for decan-3-ol than that for decan-1-ol, whereas the experiments give a larger difference between the two secondary alcohols than between decan-2-ol and decan-1-ol. Despite these discrepancies, the trends for the different alcohols are reproduced satisfactorily, suggesting that our simulation approach can be used to screen solvents for extraction and draw accurate conclusions about which solvents are more effective.

While the use of K_{DE} and α is common in the description of ethanol extraction solvents, a more general quantity that is frequently encountered in the study of partitioning is the Gibbs free energy of transfer which can be obtained from[35,36]

$$\Delta G_{trans} = -RT \ln \frac{\rho_{organic}(X)}{\rho_{aqueous}(X)}$$

where R is the gas constant, T is the absolute temperature, and $\rho_{organic}$ and $\rho_{aqueous}$ are the number densities of ethanol in the organic and aqueous phases, respectively. The Gibbs free energies of transfer for water and ethanol have been computed from the simulations and are listed in Table 1.

In general, the ΔG_{trans} values are positive (indicating a preference for the aqueous phase) for both ethanol and water, but those for water are about 8 kJ/mol larger than for ethanol. The trends in the ΔG_{trans} values for ethanol match fairly closely with those observed for K_{DE}, with transfer to the organic phase becoming more unfavorable along the series decan-1-ol to decan-4-ol and going from 2M2N to 37DM3O and 4P4H. The placement of the transfer free energies for the branched alcohols with respect to the linear alcohols is slightly different, but these differences are within the range of the statistical uncertainties.

The trends in the transfer free energies for water match well with what would be expected from the selectivity values. As decan-1-ol has the lowest selectivity, the ΔG_{trans} for water is also the lowest for this solvent. The transfer free energies increase with α going from decan-1-ol to decan-4-ol, and the values for the branched alcohols agree also quite well with the trends in α.

Table 1. Gibbs Free Energies of Transfer for Ethanol and Water from the Aqueous to the Organic Phase (with Standard Errors of the Mean), and the Average Number of Molecules and Mass of Ethanol/Water Clusters

Extractant	ΔG_{trans}(E) [kJ/mol]	ΔG_{trans}(W) [kJ/mol]	N_{clust}	M_{clust} [g/mol]
Decan-1-ol	0.34 + 0.14	8.02 + 0.13	3.1	99
Decan-2-ol	0.58 + 0.14	9.75 + 0.19	2.1	77
Decan-3-ol	0.36 + 0.13	9.96 + 0.13	2.0	74
Decan-4-ol	0.94 + 0.12	10.81 + 0.18	1.8	68
2M2N	0.91 + 0.12	9.24 + 0.10	2.3	78
37DM3O	1.11 + 0.12	9.80 + 0.09	2.0	71
4P4H	1.57 + 0.18	10.84 + 0.15	1.7	64

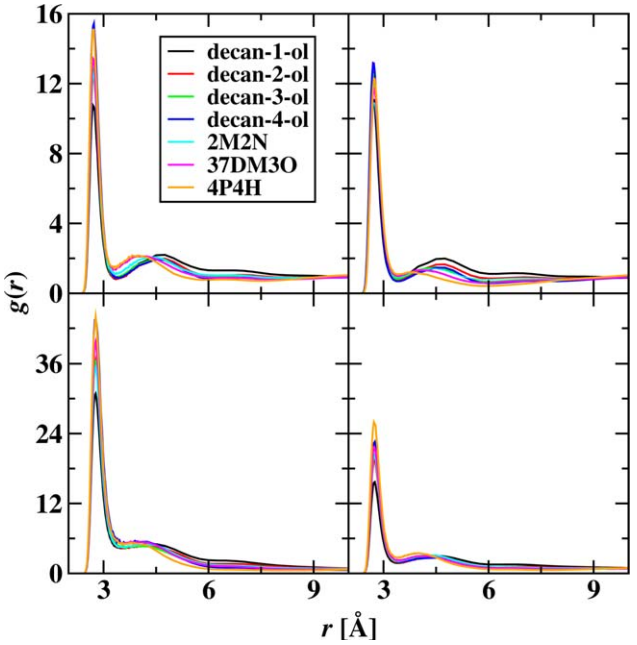

Figure 2. Oxygen-oxygen RDFs for ethanol/ethanol (top left), ethanol/solvent (top right), water/water (bottom left), and ethanol/water (bottom right).

[Color figure can be viewed in the online issue, which is available at wileyonlinelibrary.com.]

In order to explain the different performance of these 10-carbon alcohols for ethanol extraction, we have calculated radial distribution functions (RDFs). As our goal here is to identify the structural characteristics leading to differences in extraction efficiency between the different solvents, our focus is on the organic phase. The oxygen-oxygen RDFs for ethanol/ethanol and for ethanol/solvent are shown in the top two panels of Figure 2. For both RDFs, there is a general trend toward increasing height of the first peak with decreasing K_{DE}. This information can be somewhat misleading, however, as the number of ethanol molecules in the organic phase for the different extraction solvents can be quite different and, due to the normalization, the height of this first peak is a strong function of the density of ethanol in that phase. The more illuminating information is at intermediate separations, from about 3–9 Å. This range typically includes the second and third solvation shells. For alcohols that have high values of K_{DE}, the RDF in this range is higher as well. This suggests that these alcohols have larger amounts of ethanol in solvation shells beyond the first for both ethanol and the solvent. This strongly implies that the solvents most effective at extracting large amounts of ethanol do promote ethanol clustering in the organic phase.

It is not surprising that this type of structure promotes the transfer of ethanol to the organic phase, as ethanol would be much more soluble in this relatively polar cluster than in the alkyl region of the solvent. However, the same structure that makes a solvent effective for extracting ethanol also makes it less selective. RDFs for water/water and ethanol/water are shown in the bottom two panels of Figure 2. The formation of water clusters in the organic phase for the same solvents that favor the formation of ethanol clusters is indicated by the higher values for the water/water RDF in the distance range corresponding to the second and third solvation shells. Furthermore, the ethanol/water RDFs suggest that these clusters contain significant amounts of both components. This is the primary reason that those alcohols showing high values of K_{DE} also tend not to be very selective for ethanol. The driving force for the extraction of ethanol is the formation of relatively polar regions in the alcohol phase, and these regions are favorable locations for both water and ethanol.

The oxygen-oxygen RDFs and corresponding number integrals for the solvent are shown in Figure 3. In general, we see a similar correlation to that observed by Stephenson et al.[15,16] with the number of oxygen atoms within the distance range corresponding to the second and third peaks matching well with trends in K_{DE} and α. Combined with the structural information for ethanol and water, it appears that the ability of the solvent to form large hydrogen-bonded aggregates with itself is necessary to stabilize large ethanol/water clusters. If it is significantly more favorable for an alcohol to form small aggregates with only a few first shell neighbors, only a few small clusters of ethanol and water can be formed, reducing K_{DE} and increasing α.

This can be confirmed by considering the size distribution of the hydrogen-bonded aggregates in the organic phase (see Figure 4), where a set of geometric criteria[37] (i.e., O••H distance being less than 2.5 Å and cosine of O−H••O being less than −0.1) was used to define an H-bond. Within an H-bonded aggregate, each molecule is required to form an H-bond to at least one other molecule in the aggregate. The aggregate size is defined to be the number of molecules in a contiguous H-bond network. The aggregate size distribution can be determined by considering all types of molecules (10-carbon alcohol, water, and ethanol) or only the solute molecules. The aggregate size distribution for the decan-1-ol phase shows the presence of very large aggregates, sometimes containing virtually all of the molecules in the simulation box. This suggests that the primary alcohols are capable of participating in H-bonds with ethanol and water without significantly disrupting the H-bonding network between those molecules. When the hydroxyl group is located nearer to the center of the chain, as in decan-3-ol and decan-4-ol, or for tertiary alcohols, the aggregate size distribution is shifted to smaller sizes, suggesting that these alcohols are less capable of forming large H-bonded aggregates. To illustrate the dramatic differences in the extent of aggregation, snapshots of the organic phase for decan-1-ol and 4P4H are shown in Figure 5. The largest H-bonded aggregate for the 1-decanol system percolates over the entire simulation box

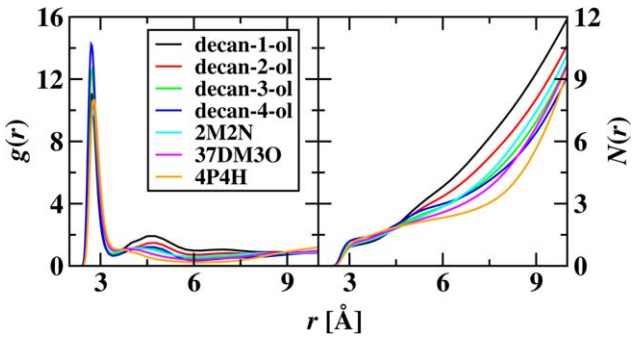

Figure 3. Oxygen-oxygen solvent/solvent RDFs (left), and number intergrals (right).

[Color figure can be viewed in the online issue, which is available at wileyonlinelibrary.com.]

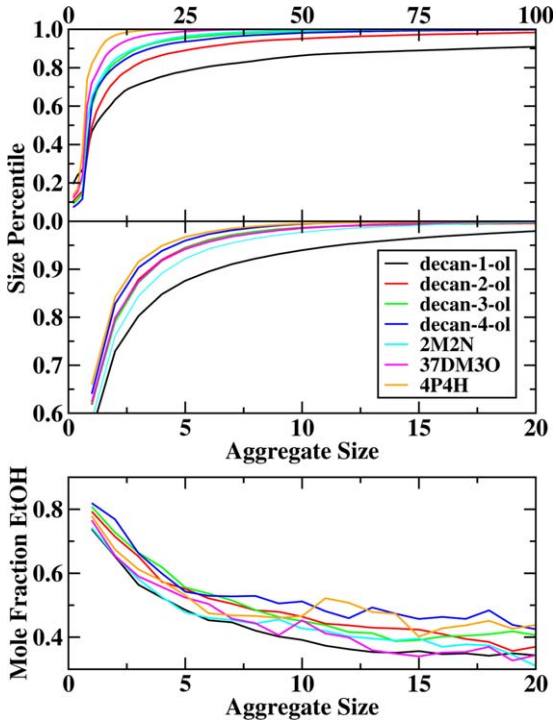

Figure 4. Aggregate size percentiles (fraction of aggregates equal to or smaller than a particular size) for all hydrogen-bonding molecules (top), and for aggregates containing only water and ethanol (middle), and ethanol mole fraction in the ethanol/water aggregates (bottom).

[Color figure can be viewed in the online issue, which is available at wileyonlinelibrary.com.]

(i.e., one might expect even larger aggregates for simulations of larger systems), whereas the much smaller H-bonded moieties in 4P4H are highly compact and well separated by alkyl-rich regions.

The formation of these clusters highlights the importance of considering this system at the finite concentrations encountered in fermentation broths. The mechanism controlling capacity and selectivity are tied to the formation of finite size ethanol/water aggregates. In general, these aggregates are not pure, well-defined, ethanol/water clusters, but rather have significant amounts of the solvent interspersed between small ethanol/water clusters. As shown in Table 1, the average size of the pure ethanol/water aggregates is quite small, containing two molecules or fewer for all but decan-1-ol.

While a general trend of high K_{DE} solvents forming large aggregates is observed, the trend in aggregate sizes does not match exactly with K_{DE}, as the tertiary alcohols tend to form smaller aggregates than any of the primary and secondary alcohols, even though they have similar K_{DE} values than decan-4-ol and also lead to larger water/ethanol aggregates. For the tertiary alcohols, while the RDFs in Figure 3 are the lowest for the branched alcohols for the second and third solvation shells, the second peak is shifted toward shorter distances and is higher than the second peak for some of the secondary alcohols. This suggests that the tertiary alcohols are forming clusters that are different in structure than those in the linear alcohols.

The middle panel of Figure 4 shows the size distribution for clusters containing only water and ethanol. Even though the branched alcohols generally form smaller aggregates overall and the RDFs suggest that these solvents lead to the formation of ethanol/water clusters of a relatively small spatial extent, the ethanol/water clusters formed in 2M2N and 37DM3O contain more molecules than those formed in decan-3-ol and decan-4-ol. As shown in the bottom panel, none of the solvent molecules have any significant preference to selectively form pure ethanol aggregates rather than ethanol/water aggregates, but overall smaller ethanol/water aggregates are significantly richer in ethanol.

Conclusions

We have demonstrated that CBMC-GEMC simulations with the TraPPE force field can predict the ability of various alcohols to extract ethanol from aqueous solution. Furthermore, we have shown that the formation of ethanol/water clusters is the primary driver for the extraction of ethanol,

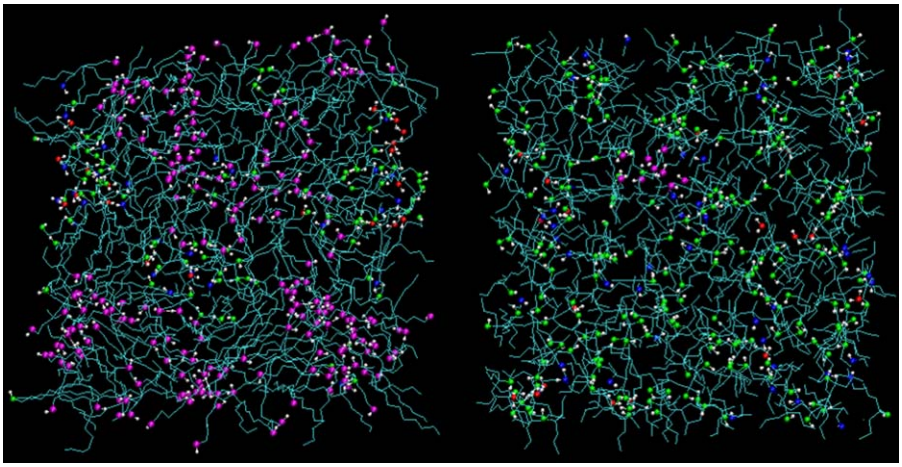

Figure 5. Snapshots of the organic phase for simulations involving decan-1-ol and 4P4H are shown on the left and right, respectively.

Carbon tails are shown as cyan lines and hydrogen atoms are shown as white spheres. Oxygen atoms in the largest cluster (regardless of molecule type), water, the 10-carbon alcohol, and ethanol are shown in magenta, red, green, and blue, respectively. [Color figure can be viewed in the online issue, which is available at wileyonlinelibrary.com.]

but that these structures also make the solvents less selective. The ability to accommodate a larger number of smaller ethanol/water clusters leads to a more efficient solvent with reasonable capacity and high selectivity.

Acknowledgments

Financial support from the National Science Foundation (CBET-0756641 and CBET-1159837) and the 3M Co. is gratefully acknowledged. Part of the computer resources was provided by the Minnesota Supercomputing Institute.

Literature Cited

1. Kamar S, Singh N, Prasad R. Anhydrous ethanol: a renewable source of energy. *Renew Sust Energ Rev*. 2010;40:1830–1844.
2. Karuppiah R, Peschel A, Grossmann IE, Martín M, Martinson W, Zullo L. Energy optimization for the design of corn-based ethanol plants. *AIChE J*. 2008;54:1499–1525.
3. Stephanopoulos G. Challenges in engineering microbes for biofuels production. *Science*. 2007;315:801–804.
4. Hill J, Nelson E, Tilman D, Polasky S, Tiffany D. Environmental, economic, and energetic costs and benefits of biodiesel and ethanol biofuels. *Proc Natl Acad Sci USA*. 2006;103:11206–11210.
5. Fanta GF, Burr RC, Orton WL, Doane WM. Liquid-phase dehydration of aqueous ethanol-gasoline mixtures. *Science*. 1980;210:646–647.
6. Hartline FF. Lowering the cost of alcohol. *Science*. 1979;206:41–42.
7. Ladisch MR, Dyck K. Dehydration of ethanol: new approach gives positive energy balance. *Science*. 1979;205:898–900.
8. Offeman RD, Stephenson SK, Robertson GH, Orts WJ. Solvent extraction of ethanol from aqueous solutions using biobased oils, alcohols, and esters. *J Am Oil Chem Soc*. 2006;83:153–157.
9. Offeman RD, Stephenson SK, Robertson GH, Orts WJ. Solvent extraction of ethanol from aqueous solutions. I. Screening methodology for solvents. *Ind Eng Chem Res*. 2005;44:6789–6796.
10. Offeman RD, Stephenson SK, Robertson GH, Orts WJ. Solvent extraction of ethanol from aqueous solutions. II. Linear, branched, and ring-containing alcohol solvents. *Ind Eng Chem Res*. 2005;44:6797–6803.
11. Egan BZ, Lee DD, McWhirter DA. Solvent extraction and recovery of ethanol from aqueous solutions. *Ind Eng Chem Res*. 1988;27:1330–1332.
12. Munson CL, King CJ. Factors Influencing solvent selection for extraction of ethanol from aqueous solutions. *Ind Eng Chem Proc Design Develop*. 1984;23:109–115.
13. Roddy JW. Distribution of ethanol-water mixtures to organic liquids. *Ind Eng Chem Proc Design Develop*. 1981;20:104–108.
14. King CJ. Separation Processes. New York, NY: McGraw-Hill; 1971.
15. Stephenson SK, Offeman RD, Robertson GH, Orts WJ. Ethanol and water capacities of alcohols: a molecular dynamics study. *Chem Eng Sci*. 2006;61:5834–5840.
16. Stephenson SK, Offeman RD, Robertson GH, Orts WJ. Hydrogen-bond networks in linear, branched, and tertiary alcohols. *Chem Eng Sci*. 2006;62:3019–3031.
17. Panagiotopoulos AZ. Direct determination of phase coexistence properties of fluids by Monte Carlo simulation in a new ensemble. *Mol Phys*. 1987;61:813–826.
18. Panagiotopoulos AZ, Quirke N, Stapleton M, Tildesley DJ. Phase equilibria by simulation in the Gibbs ensemble. Alternative derivation, generalization, and application to mixture and membrane equlibria. *Mol Phys*. 1988;63:527–545.
19. Smit B, Desmedt P, Frenkel D. Computer simulations in the Gibbs ensemble. *Mol Phys*. 1989;68:931–950.
20. Siepmann JI, Frenkel D. Configurational-bias Monte Carlo. A new sampling scheme for flexible chains. *Mol Phys*. 1992;75:59–70.
21. Mooij GCAM, Frenkel D, Smit B. Direct simulation of phase equilibria of chain molecules. *J Phys Cond Matt*. 1992;4:L255–L259.
22. Laso M, DePablo JJ, Suter UW. Simulation of phase equilibria for chain molecules. *J Chem Phys*. 1992;97:2817–2819.
23. Martin MG, Siepmann JI. Novel configurational-bias Monte Carlo method for branched molecules. Transferable potentials for phase equilibria. 2. United-atom description of branched alkanes. *J Phys Chem. B*. 1999;103:4508–4517.
24. Chen B, Siepmann JI. Partitioning of alkane and alcohol solutes between water and (dry or wet) 1-octanol. *J Am Chem Soc*. 2000;122:6464–6467.
25. Rafferty JL, Zhang L, Siepmann JI, Schure MR. Retention mechanism in reversed-phase liquid chromatography: a molecular perspective. *Anal Chem*. 2007;79:6551–6558.
26. Siepmann JI, McDonald IR. Monte Carlo simulations of mixed monolayers. *Mol Phys*. 1992;75:255–259.
27. Martin MG, Siepmann JI. Predicting multicomponent phase equilibria and free energies of transfer for alkanes by molecular simulation. *J Am Chem Soc*. 1997;119:8921–8924.
28. Jorgensen WL, Chandrasekhar J, Madura JD, Impey RW, Klein ML. Comparison of simple potential functions for simulating liquid water. *J Chem Phys*. 1983;79:926–935.
29. Martin MG, Siepmann JI. Transferable potentials for phase equilibria. 1. United-atom description of n-alkanes. *J Phys Chem B*. 1999;103:4508–4517.
30. Chen B, Potoff JJ, Siepmann JI. Monte Carlo calculations for alcohols and their mixtures with alkanes. Transferable potentials for phase equilibria. 5. United-atom description of primary, secondary, and tertiary alcohols. *J Phys Chem B*. 2001;105:3093–3104.
31. Chen B, Siepmann JI. Microscopic structure and solvation in dry and wet octanol. *J Phys Chem B*. 2006;110:3555–3563.
32. Garrido NM, Queimada AJ, Jorge M, Macedo EA, Economou IG. 1-Octanol/water partition coefficients of n-alkanes from molecular simulations of absolute solvation free energies. *J Chem Theory Comput*. 2009;5:2436–2446.
33. Rafferty JL, Siepmann JI, Schure MR. Investigating the driving forces for retention in reversed-phase liquid chromatography: Monte Carlo simulations of solute partitioning between n-hexadecane and various aqueous-organic mixtures. *Fluid Phase Equil*. 2010;290:25–35.
34. Allen MP, Tildesley DJ. Computer Simulation of Liquids.New York: Oxford University Press; 1987.
35. Ben-Naim A. Statistical Thermodynamics for Chemists and Biochemists. New York: Plenum Press; 1992.
36. Martin MG, Siepmann JI. Calculating Gibbs free energies of transfer from Gibbs ensemble Monte Carlo simulations. *Theor Chem Acc*. 1998;99:347–350.
37. Stubbs JM, Siepmann JI. Elucidating the vibrational spectra of hydrogen-bonded aggregates in solution: electronic structure calculations with implicit solvent and first principles molecular dynamics simulations with explicit solvent for 1-hexanol in n-hexane. *J Am Chem Soc*. 2005;127:4722–4729.

Manuscript received Aug. 5, 2012, and revision received Jan. 5, 2013.